Broadly tunable laser operation near 2 μm in a locally disordered crystal of Tm^{3+}-doped $NaGd(WO_4)_2$

José M. Cano-Torres, María Dolores Serrano, and Carlos Zaldo

Instituto de Ciencia de Materiales de Madrid, Consejo Superior de Investigaciones Científicas, c/ Sor Juana Inés de la Cruz 3, Cantoblanco, E-28049 Madrid, Spain

Mauricio Rico, Xavier Mateos, Junhai Liu, Uwe Griebner, and Valentin Petrov

Max-Born-Institute for Nonlinear Optics and Ultrafast Spectroscopy, 2A Max-Born-Strasse, D-12489 Berlin, Germany

Francisco José Valle

Instituto de Cerámica y Vidrio, Consejo Superior de Investigaciones Científicas, c/ Kelsen 5, Cantoblanco, E-28049 Madrid, Spain

Miguel Galán and Gregorio Viera

Monocrom SL, c/ Vilanoveta 6, E-08800, Vilanova i la Geltrú, Spain

Received March 29, 2006; accepted July 3, 2006; posted July 31, 2006 (Doc. ID 69459)

Output powers as high as 300 mW were obtained at 1925 nm in the cw regime with a Tm laser operating at room temperature, either with Ti-sapphire or diode laser pumping, using a new single crystal of $NaGd(WO_4)_2$ grown by the Czochralski method and doped with 5 mol.% of Tm^{3+} in the melt. This crystal belongs to the $I\bar{4}$ tetragonal space group and exhibits a locally disordered structure due to the random occupancy of the same lattice sites by Na and Gd (or Tm) ions. The local disorder results in large bandwidths of the Tm^{3+} optical transitions (e.g., FWHM $\approx 60\ \mathrm{cm}^{-1}$ at 5 K for the $^3H_6 \rightarrow {}^3F_4$ transition involved in the laser emission), which allows one to obtain one of the broadest laser tunability ranges, from 1813 to 2025 nm ($\approx$17 THz), achieved with a Tm^{3+}-doped crystalline material. A detailed characterization of the Tm^{3+} optical spectroscopy in this novel host was performed at 5 and 300 K. © 2006 Optical Society of America

OCIS codes: 140.3380, 140.5680, 140.3480, 140.3070, 140.3580, 140.3600.

1. INTRODUCTION

Laser radiation in the 2 μm spectral range is useful for different applications related to its eye-safe nature in medicine[1] and environmental gas detection.[2] The basis for most of these applications is the strong optical absorption in the 1.9–2.0 μm region of water, either liquid or vapor, and some gases such as NO_2, CO_2, and NH_3. Broad wavelength tunability is needed to realize devices capable of analyzing all these compounds with a single laser source. Alternative compact and tunable sources exist, e.g., based on strained-InGaAs/InP laser diodes, but their power level (e.g., 2.2 mW in Ref. 2) is quite low. Solid-state lasers can also potentially provide much larger spectral ranges of tunability. Although traditionally solid-state lasers operating near 2 μm were based on Ho^{3+}-doped crystals,[3] the new optical pump technologies with robust AlGaAs laser diodes have promoted intense activity for the search of suitable materials for all-solid-state laser systems efficiently pumped near 800 nm and operating on the $^3F_4 \rightarrow {}^3H_6$ Tm^{3+} transition.

The $4f^n$ configurations of trivalent lanthanides, including the $4f^{12}$ of Tm^{3+}, are shielded from the crystal field of the host ligands by outer 5*s* and 5*p* electrons, therefore the coupling to the vibronic environment is relatively weak. As a consequence the bandwidths of the electronic transitions are narrow and the laser tunability is limited. In some cases, however, the phonon broadening is larger and laser tuning from 1.87 to 2.16 μm and from 1.85 to 2.14 μm has been demonstrated with the cubic oxides Tm:YAG and Tm:YSGG, respectively.[4] Further broadening of the spectral features can be expected for solids with multisites, defects, or local disorder. The use of glasses as laser hosts, particularly at high power levels, is limited by their poor thermal properties. Recently there were some attempts to study multisite fluorites, which are characterized by low phonon energies and hence long lifetime of the metastable levels, for room-temperature cw laser operation. Thus tuning between 1835 and 1970 nm was demonstrated with $Tm:CaF_2$,[5] while the initial results with $Tm:KYF_4$ were modest—only narrow tunability between 2010 and 2022 nm was achieved.[6]

The disordered tetragonal crystal $NaGd(WO_4)_2$

(NaGdW) was used as a host of the Nd^{3+} ion as early as 1964.[7] This compound belongs to a more general class $NaT(WO_4)_2$, where T is a trivalent cation, either Al, Ga, In, Cr, Bi, Y, La, or a lanthanide Ln^{3+}=Ce-Lu. As shown recently, the spectral broadening in such double tungstates is related not only to the random distribution of Na and T cations but also to the existence of two lattice sites for the T cations because the refined crystalline structure has a symmetry of $I\bar{4}$.[8] Recently, our group achieved laser operation of Yb^{3+}:NaGdW demonstrating simultaneous tunability from 1016 to 1049 nm.[9] The present work is devoted to the growth, spectroscopic properties, and laser demonstrations of Tm:NaGdW. Previously, spectroscopic investigations related to the $^3F_4 \rightarrow {}^3H_6$ Tm^{3+} transition appeared for some related disordered double tungstates and molybdates: $KLa(WO_4)_2$,[10] $NaBi(WO_4)_2$,[11] $NaLa(MoO_4)_2$,[12] and $KLa(MoO_4)_2$.[13] However, to the best of our knowledge, Tm^{3+} lasing has not been reported for such disordered crystal hosts. Here we demonstrate broadly tunable cw laser operation of Tm^{3+} in NaGdW under Ti:sapphire and diode pumping.

2. CRYSTAL GROWTH AND STRUCTURAL STUDIES

NaGdW crystals grown by the Czochralski method have the crystal structure symmetry of the noncentrosymmetric tetragonal space group $I\bar{4}$ where Na^+ and Gd^{3+} reside in two nonequivalent 2*b* and 2*d* lattice sites, both with local S_4 point symmetry if all ligands of a given site are either only Na^+ or Gd^{3+}.[8] Since tetragonal structure has been reported also for $NaTm(WO_4)_2$,[14] it can be expected that Tm:NaGdW is isostructural with NaGdW, but the incongruent melting reported for $NaTm(WO_4)_2$ (Ref. 14) suggests that the Tm incorporation will be limited to a certain Tm doping level. We grew a single crystal of $NaGd_{1-x}Tm_x(WO_4)_2$ with $x_{MELT}=0.05$ by the Czochralski technique using pulling equipment with crystal diameter control. The starting materials were Alfa Aesar 99.99% Gd_2O_3, 99.99% Tm_2O_3, 99.5% Na_2CO_3, and 99.8% WO_3. The stoichiometric composition was melted in a 75 cm^3 Pt crucible with the addition of 1.3 mol.% of $Na_2W_2O_7$ to slightly decrease the melting temperature of the mixture and to partially compensate for Na and W evaporation.

After homogenization of the melt for 3 h at a temperature 25 °C above the melting point (≈1265 °C for NaGdW), the optimum crystallization temperature was determined by monitoring the crucible weight when seeding with *c*-oriented NaGdW. The rotation and pulling rates were 10 rpm and 1 mm/h, respectively. The grown crystal was cooled down to room temperature at a rate of 10 °C/h. The crystal dimensions were ~20 mm in diameter and 50 mm in length. Although the crystal was transparent, it exhibited some optical gradients with a period of ~1 mm along the growth axis. Such gradients also appeared in some of our undoped NaGdW crystals and we believe they are likely related to small (<0.2 °C) temperature fluctuations during the growth process leading to composition modulation and the corresponding refractive index change. These gradients do not significantly affect the Tm incorporation or its spectroscopic properties. The tetragonal structure of the grown crystal was confirmed by x-ray powder diffraction.

The Tm and Gd concentrations in the crystal were determined by using Philips x-ray fluorescence equipment, model MagiX Super Q, with a 2.4 kW Rh x-ray generator. For both ions the $L_{\alpha 1}$ x-ray emission lines were scanned by a LiF 200 crystal analyzer using a narrow (150 μm) collimator. For the analysis, 0.3 g of $NaGd_{1-x}Tm_x(WO_4)_2$ were melted with 5.5 g of $Li_2B_4O_7$ to avoid particle size effects. Previously a calibration curve was prepared using standards of Na_2CO_3, Gd_2O_3, Tm_2O_3, and WO_3 mixtures, also melted with $Li_2B_4O_7$. The composition deduced from these measurements is $Na_{1-\delta}Gd_{1.07}Tm_{0.037}(W_{1-\gamma}O_4)_2$. We note that the total content of trivalent ions, Gd and Tm, is larger than the $x=1$ expected from the nominal formula and this must be compensated by some deficiency of Na and W ions (δ and γ parameters, respectively). Qualitatively similar results were obtained from single-crystal x-ray diffraction analysis of NaGdW grown by the Czochralski method.[8] These Na and W deficiencies are due to the high Na and W volatilities, which after resolidification form $Na_xWO_3 (x<1)$ compounds on the pulling rod. The obtained segregation coefficient of Tm is $K = [Tm]_{crystal}/[Tm]_{melt} = 0.7$. Taking into account the cell volume of NaGdW, $V = 312.9$ Å^3,[8] the Tm density in the crystal amounts to $[Tm]_{crystal} = 2.34 \times 10^{20}$ cm^{-3}.

Samples for spectroscopy and laser experiments were oriented by the Laue x-ray diffraction technique and polished to optical grade to obtain scratch-free and λ/10 surface flatness, with face parallelism better than 10 arc min.

3. Tm^{3+} SPECTROSCOPY IN NaGdW

The optical absorption (OA) measurements were performed with a Varian spectrophotometer, Model Cary 5E. The photoluminescence (PL) was excited by a Ti:sapphire laser. The emission was dispersed by a SPEX 340E spectrometer (f=34 cm) and detected with a 77 K cooled InSb photovoltaic detector (Hamamatsu, Model P5968-060). The detector signal was recorded with a lock-in amplifier. The sample temperature was varied in the 5–300 K range using a close-cycle He cryostat.

A. 5 K Optical Spectroscopy

Figure 1 shows the 5 K ground-state optical absorption (GSA) for $^3H_6 \rightarrow {}^{2S+1}L_J$ transitions of Tm^{3+} in NaGdW. Some of the Tm^{3+} multiplets have a mixed configuration character[15]; for instance, $^3F_4$ is strongly mixed with $^1G_4$, $^3H_4$ with $^3F_4$, $^3F_2$ with $^1D_2$, and $^1G_4$ with $^3H_4$, but it is still preferable to use simple labels to refer to these multiplets. Despite the disordered character of the host, the intensity of the spectral bands depends strongly on the polarization. Following the standard spectroscopic notation for uniaxial crystals, the spectra are labeled as $\alpha(\boldsymbol{E} \perp \boldsymbol{c}, \boldsymbol{H} \perp \boldsymbol{c})$, $\pi(\boldsymbol{E} \parallel \boldsymbol{c})$, and $\sigma(\boldsymbol{H} \parallel \boldsymbol{c})$. The $^3F_4 \rightarrow {}^3H_6$ PL spectrum that is also included in Fig. 1 exhibits a pronounced polarization dependence. Further assessment of the first Stark levels of the ground $^3H_6$ multiplet was inferred from the 5–300 K thermal evolution of OA (not shown for the sake of brevity). The Stark levels of the

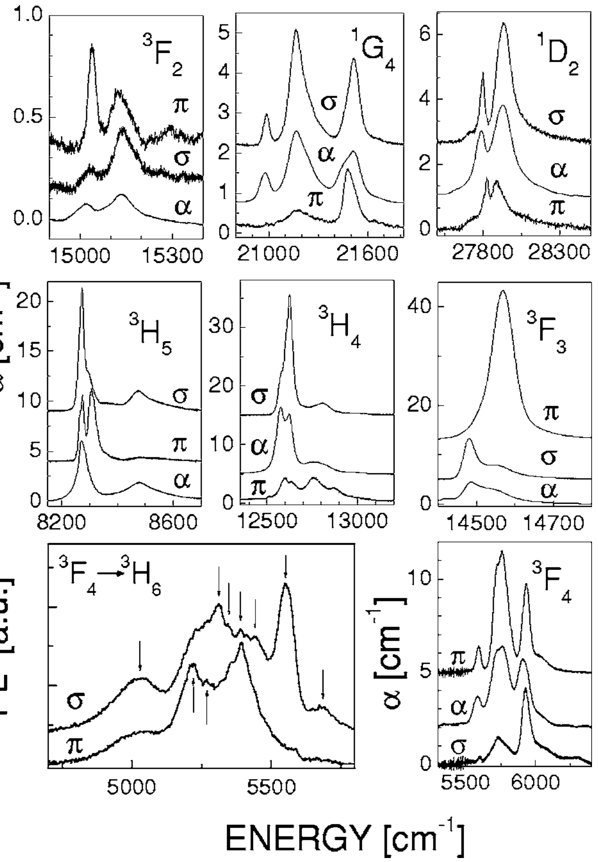

Fig. 1. Low-temperature (5 K) polarized (α, σ, and π) OA coefficient α and PL of Tm:NaGdW. The PL was excited at 792.1 and 793.5 nm for the σ and π spectra, respectively.

Table 1. Observed Stark Energy Levels (in cm^{-1}) of Tm^{3+} in NaGdW, Number of Irreducible Representations (Γ_1, Γ_2, or $\Gamma_{3,4}$) Expected for Each $^{2S+1}L_J$ Multiplet in the S_4 Symmetry[a]

$^{2S+1}L_J$	Energy (cm^{-1})	$\Gamma_1+\Gamma_2$, $\Gamma_{3,4}$
$^3H_6$	0, $60^{\#}$, 132^{*}, 246^{*}, $270^{\#*}$, $291^{\#*}$, $373^{\#*}$, 419^{*}, 465^{*}, 660^{*}	7, 3
$^3F_4(^1G_4)$	5596, 5731, 5759, 5934, 5028	5, 2
$^3H_5$	8267, 8274, 8297, 8308, 8476	5, 3
$^3H_4(^3F_4)$	12,576, 12,601, 12,626, 12,636, 12,757, 12,811, 12,876	5, 2
$^3F_3$	14,481, 14,553, 14,571	3, 2
$^3F_2(^1D_2)$	15,039, 15,135	3, 1
$^1G_4(^3H_4)$	20,989, 21,165, 21,480, 21,517	5, 2
$^1D_2$	27,800, 27,827, 27,889, 27,937	3, 1

[a] $^3H_6$ levels obtained from 5–300 K OA measurements (#) and obtained from PL measurements (*).

ground and excited Tm^{3+} multiplets determined from these measurements are summarized in Table 1. Taking into account that Tm^{3+} resides in the two nonequivalent 2*b* and 2*d* sites of the lattice and that each of these sites has several environments related to the actual Na$^+$ and Gd^{3+} distributions, these assignments must be understood as corresponding to an average Tm^{3+} center. The presence of the environmental ionic distributions might be related to a reduction of the local symmetry with respect to the S_4 host site symmetry; however, we shall use the host symmetry as a first approximation in the analysis of the polarized spectra. For most of the excited multiplets the number of experimentally resolved bands is lower than the maximum $2J+1$ multiplet multiplicity. This fact could be attributed to limitations of the experimental results or to a ground Stark level $^3H_6(0)$ belonging to the Γ_1 or Γ_2 irreducible representations of the S_4 point group (see Table 2).

The $^3P_0$ Tm^{3+} multiplet having a unique Γ_1 irreducible representation typically peaks above 34,000 cm^{-1} and in the present case this absorption band overlaps the ultraviolet OA edge of NaGdW ($\approx$33,900 cm^{-1}). Therefore, the assignment of the Stark levels of Table 1 to specific irreducible representations based on the polarization rules observed is not possible. It must be noted that, although not identical, the 5 K σ and α spectra shown in Fig. 1 are rather similar to each other and quite different from the π spectrum, also shown in Fig. 1. Thus, according to the selection rules of the S_4 point symmetry (see Table 2), the observed transitions are electric dipole (ED). This conclusion holds even for the $^3H_6 \rightarrow ^3H_5$ transition ($\Delta J=1$) for which some magnetic dipole (MD) contribution is expected. However, it must be recognized that the S_4 point-group symmetry of the host cannot fully describe the Tm^{3+} symmetry in NaGdW: First, the 5 K σ and α spectra are not identical, and second, and more important, some of the OA bands (e.g., 15,135 cm^{-1} for $^3F_2$ or 5934 cm^{-1} for $^3F_4$) are seen with similar intensities in the σ and π spectra, which is forbidden according to the selection rules of the S_4 symmetry (see Table 2). These observations are indicative of a reduction of the Tm^{3+} local site symmetry. Similar site symmetry reductions have been obtained previously for Pr^{3+} and Nd^{3+} in tetragonal NaBi(WO$_4$)$_2$ single crystals.[16] They can be qualitatively attributed to the coexistence of several Tm^{3+} centers occurring as a result of the random distribution of Na$^+$ and Gd^{3+} ions as first cationic neighbors of Tm^{3+} in the 2*b* and 2*d* sites.

The ground-state $^3H_6$ splitting of Tm^{3+} in NaGdW is relatively large and comparable to that of Tm:YAG.[17] This means less thermal population of the lower laser level for the $^3F_4 \rightarrow ^3H_6$ transition and operation as a quasi-four-level system.

B. 300 K Optical Spectroscopy

Figure 2 shows the GSA cross sections ($\sigma_{\text{GSA}} = \alpha/[\text{Tm}]_{\text{crystal}}$ where α is the OA coefficient) for the $^3H_6 \rightarrow ^3H_4$ transition recorded at 300 K. These bands match rather well the emission spectrum of AlGaAs diode lasers. The α and σ spectra have very similar peak values and

Table 2. Polarization Rules for the S_4 Site Symmetry and J Whole[a]

	ED			MD		
IR	Γ_1	Γ_2	$\Gamma_{3,4}$	Γ_1	Γ_2	$\Gamma_{3,4}$
Γ_1	—	π	α,σ	σ	—	α,π
Γ_2	π	—	α,σ	—	σ	α,π
$\Gamma_{3,4}$	α,σ	α,σ	π	α,π	α,π	σ

[a] Irreducible representations (IR) ($\Gamma_1,\Gamma_2,\Gamma_{3,4}$) and experimental spectra (α,σ,π).

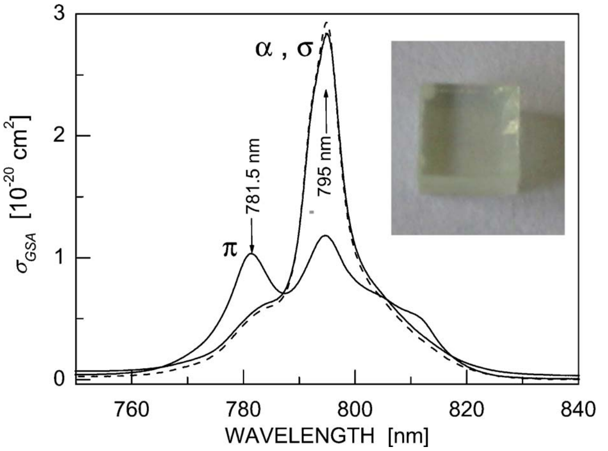

Fig. 2. (Color online) Ground-state $^3H_4$ absorption cross sections σ_{GSA} of Tm:NaGdW at 300 K for α (dashed curve), σ and π (solid curves) configurations. The inset shows an ≈3 mm × 3 mm × 3 mm sample used in the laser experiments.

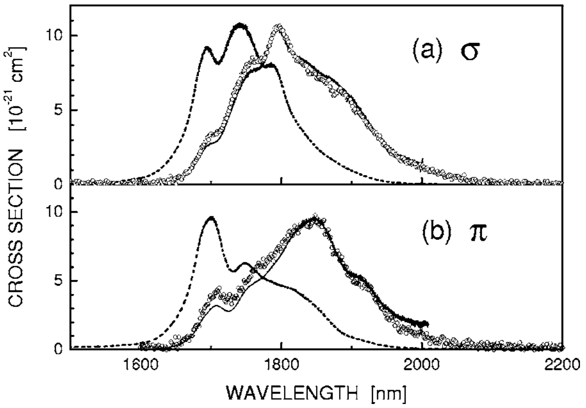

Fig. 3. $^3H_6 \leftrightarrow {}^3F_4$ ground-state absorption cross section (dashed curves) and emission cross section at 300 K calculated by the reciprocity method (solid curves) of Tm:NaGdW. The experimental PL excited at 795 nm (points) is shown for comparison. (a) σ configuration, (b) π configuration.

spectral shapes. In both cases the maximum absorption cross sections exceed by a factor of more than 2 the cross section for the π polarization at the same peak wavelength, 795 nm. The maximum cross sections at this wavelength are $\sigma_{\mathrm{GSA}}(\sigma) \approx \sigma_{\mathrm{GSA}}(\alpha) = 2.9 \times 10^{-20}$ cm^2 and $\sigma_{\mathrm{GSA}}(\pi) = 1.18 \times 10^{-20}$ cm^2. The FWHM of the more intense σ and α absorption lines is ~8 nm, which relaxes the requirements for pumping with diode lasers.

After excitation of the $^3H_4$ manifold, energy transfer by the cross-relaxation process $^3H_4 + {}^3H_6 \rightarrow 2\,{}^3F_4$ can contribute to the population of the $^3F_4$ upper laser level for the 2 μm emission of Tm^{3+}. Figure 3 shows the calculated room-temperature emission cross section σ_{EMI} for the $^3F_4 \rightarrow {}^3H_6$ laser transition using the reciprocity method[18]:

$$\sigma_{\mathrm{EMI}} = \sigma_{\mathrm{GSA}} \frac{Z_l}{Z_u} e^{(E_{zl}-h\nu)/k_B T}, \qquad (1)$$

where Z_u and Z_l [$Z = \Sigma_k \exp(-E_k/k_B T)$] are the partition functions of the upper and lower multiplets, respectively; E_{zl} is the energy difference between the lowest Stark levels of both multiplets; k_B is the Boltzman constant; and T is the temperature. The values $E_{zl} = 0.6939$ eV and $Z_l/Z_u = 1.228$ were obtained from the energy-level data given in Table 1. The calculated σ_{EMI} agrees rather well with the experimentally recorded PL profiles. The maximum emission cross sections are $\sigma_{\mathrm{EMI}}(\sigma) = 10.6 \times 10^{-21}$ cm^2 at 1796 nm and $\sigma_{\mathrm{EMI}}(\pi) = 9.5 \times 10^{-21}$ cm^2 at 1847 nm.

The gain cross section can be expressed as $\sigma_{\mathrm{GAIN}}(\lambda) = \beta \sigma_{\mathrm{EMI}}(\lambda) - (1-\beta)\sigma_{\mathrm{GSA}}(\lambda)$, where β represents the ratio of the Tm ions in the excited state to the total ion density. σ_{GAIN} is plotted in Fig. 4 for both polarizations and indicates the expected oscillation wavelength in the absence of frequency-selective elements in the laser cavity.

The radiative lifetime τ_{rad} can be calculated by the Fuechtbauer–Ladenburg method as

$$\tau_{\mathrm{rad}} = \frac{1}{8\pi n^2 c}\left[\int \frac{\langle \sigma(\lambda) \rangle}{\lambda^4} \mathrm{d}\lambda \right]^{-1}.$$

Using an average $(2\sigma + \pi)/3$ of the results of Fig. 3, $\tau_{\mathrm{rad}} = 2385$ μs is obtained for the $^3F_4$ Tm^{3+} multiplet.

Alternatively the Judd–Ofelt formalism based on the 300 K integrated OA Γ provides detailed information on the transition probability A, branching ratios β_{ij}, and radiative lifetime τ_{rad} of different deexcitation transitions. The method has been developed in detail previously.[19] For Tm^{3+} we used the reduced matrix elements given by Carnall *et al.*,[20] and the Γ/[Tm] values determined for σ and π polarization are given in Table 3. The experimental ED oscillator strengths $f_{\mathrm{ED,exp}}$ were obtained after $(2\sigma + \pi)/3$ average of the experimental data and after subtraction of the MD oscillator strength calculated for $^3H_6 \rightarrow {}^3H_5$, f_{MD}. The NaGdW refractive indices for each wavelength were used.[8] The fitting produces the following Judd–Ofelt parameter set: $\Omega_2 = 9.48 \times 10^{-20}$ cm^2, $\Omega_4 = 1.28 \times 10^{-20}$ cm^2, and $\Omega_6 = 1.36 \times 10^{-20}$ cm^2 with a root-mean-square deviation $\Delta f = 0.65 \times 10^6$. The fluorescence properties obtained using this Ω_k set are summarized in Table 4. The $^3F_4$ radiative lifetime obtained by this method is $\tau_{\mathrm{rad}} = 1790$ μs. The differences of the $^3F_4$ τ_{rad} obtained by the Fuechtbauer–Ladenburg method and by the Judd–Ofelt formalism are due to the experimental uncertainties as well as to the use of approximated reduced matrix elements for Tm^{3+}.

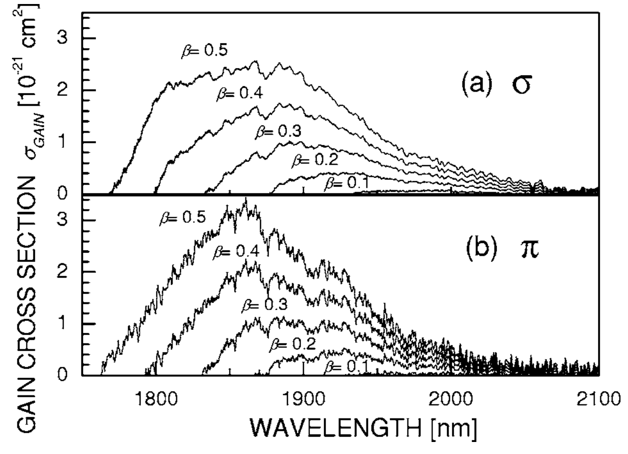

Fig. 4. $^3F_4 \rightarrow {}^3H_6$ gain cross section $\sigma_{\mathrm{GAIN}}(\lambda)$ of Tm:NaGdW for several inversion rates β.

Table 3. Average Wavelength $\bar{\lambda}$, Integrated OA Cross Sections Γ/[Tm], Averaged ED Oscillator Strength $\bar{f}_{\mathrm{ED,exp}}$, and Calculated ED Oscillator Strength $f_{\mathrm{ED,cal}}$ for $^{2S+1}L_J$ Multiplets of Tm^{3+} in $NaGd(WO_4)_2$

$^3H_6\rightarrow$	$\bar{\lambda}$ (nm)	Γ_σ/[Tm] (10^{-27} cm^3)	Γ_π/[Tm] (10^{-27} cm^3)	$\bar{f}_{\mathrm{ED.exp}}$ ($\times10^8$)	$\bar{f}_{\mathrm{ED.cal}}$ ($\times10^8$)
$^1D_2$	360	3.81	4.06	339	255
$^1G_4$	471	5.54	4.61	266	202
$^3F_2$+$^3F_3$	688	12.76	27.58	423	447
$^3H_4$	795	40.54	36.38	700	675
$^3H_5$	1210	38.73	36.95	294[a]	286
$^3F_4$	1745	158.37	133.24	557	564

[a] The following MD contributions f_{MD} were evaluated and subtracted from the experimental results: σ, 0.6374×10^{-6}; π, 0.6375×10^{-6}.

Table 4. ED and MD Transition Probabilities A_{ED} and A_{MD}; Branching Ratios β_{ij} and Radiative Lifetimes τ_{rad} of Tm^{3+} in $NaGd(WO_4)_2$ Calculated from the $\Omega_2=9.48\times10^{-20}$ cm^2, $\Omega_4=1.28\times10^{-20}$ cm^2, $\Omega_6=1.36\times10^{-20}$ cm^2 Set[a]

Transition	λ (nm)	$A_{\mathrm{ED}}+A_{\mathrm{MD}}$ (s^{-1})	β_{ij} (%)	τ_{rad} (μs)
$^1D_2\rightarrow{}^3H_4$	658	20,955	34	16
$^3F_4$	452	19,164	31	
$^3H_6$	363	14,097	23	
$^1G_4\rightarrow{}^3F_4$	648	4502	46	102
$^3H_6$	480	3307	34	
$^3F_2\rightarrow{}^3F_4$	1078	2526	61	242
$^3H_6$	681	1203	29	
$^3F_3\rightarrow{}^3H_5$	1599	1154	21	182
$^3H_6$	705	3412	64	
$^3H_4\rightarrow{}^3H_6$	811	3703	89	241
$^3H_5\rightarrow{}^3H_6$	1260	514+97	99	1623
$^3F_4\rightarrow{}^3H_6$	1853	559	100	1790

[a] Only transitions with $\beta_{ij}>20\%$ are shown.

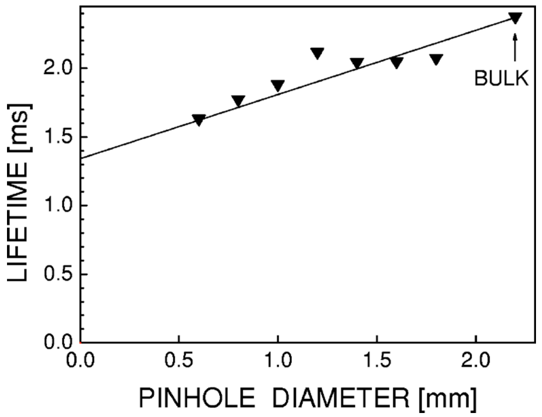

Fig. 5. Fluorescence lifetime of the metastable $^3F_4$ level of Tm^{3+} in $NaGd(WO_4)_2$ measured at room temperature by the pinhole method.

The standard procedures for lifetime measurement of transitions ending at the ground multiplet often yield unrealistically large values due to radiation trapping. To avoid this, the $^3F_4$ lifetime was evaluated by the pinhole method, which eliminates to a great extent the reabsorption effect.[21] Figure 5 shows the results obtained by excitation at 796 nm with a nanosecond optical parametric oscillator and detection of the fluorescence at 1710 nm. It is clear that the lifetime measured without a pinhole (bulk) is longer. The extrapolation for zero diameter of the pinhole gives a lifetime of 1.35±0.20 ms for this Tm doping level ($x=0.037$ in the crystal).

This measured lifetime of the $^3F_4$ metastable level of Tm^{3+} in $NaGd(WO_4)_2$ falls into the range of values reported for other double tungstate and molybdate hosts at 300 K. Using the same method, a lifetime of 0.9 ms was obtained for 5 mol.% Tm-doped $KGd(WO_4)_2$ and $KLu(WO_4)_2$ and 1.34 ms for 3 mol.% Tm-doped $KLu(WO_4)_2$, which are monoclinic ordered crystals.[22] Some values were reported also for disordered double tungstates and molybdates, e.g., 1.6 ms for $KLa(MoO_4)_2$ (Ref. 13) and 1.68 ms for $KLa(WO_4)_2$,[10] but in these cases the radiation trapping effect was not taken into account and the lifetimes were probably overestimated.

4. LASER OPERATION

A. Ti:sapphire Pumping

We first tested Tm:NaGdW for laser operation using a tunable cw Ti:sapphire laser with an output linewidth of ≈0.2 nm and a maximum output power of 3 W near 800 nm. The astigmatically compensated *X*-type cavity with a total length of 90 cm is shown in Fig. 6. M1, M2, and M3 were highly reflecting (>99.9%) from 1800 to 2075 nm and antireflection coated on the rear side for high transmission from 780 to 1020 nm. Output couplers (M4 in the figure) with transmission $T_{\mathrm{OC}}=1.5\%$, 3%, 5%, and 10% were used. A single-plate intracavity Lyot filter was employed for tuning. We used an *a*-cut sample that allows us to orient the crystal *c* axis either perpendicular (σ) to the pump beam polarization or in the same plane (π). The uncoated Tm:NaGdW sample (inset Fig. 2) was positioned under Brewster's angle that determines the laser polarization, and the pump polarization was always in the same plane. In the position of the Tm crystal, the pump spot had a Gaussian waist of 37 μm. The sample was clamped in a copper block and the temperature was maintained at 10 °C with water cooling.

The Ti:sapphire laser was tuned to the peak of the $^3H_4$ absorption band (see Fig. 2). The optimum pump wavelength was found at 795.5 and 795.6 nm for the σ and π

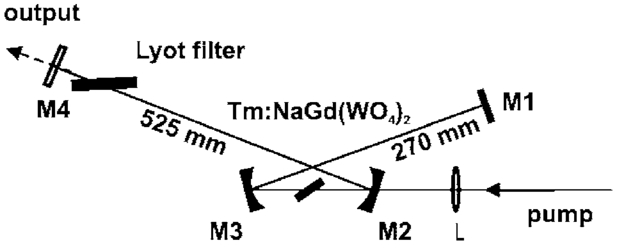

Fig. 6. Cavity setup of the Tm:NaGdW laser with Ti:sapphire laser pumping. L, antireflection-coated focusing lens with $f=70$ mm; M1, plane total reflector; M2–M3, mirrors with radius of curvature of −100 mm; M4, plane output coupler. For tuning experiments, a single-plate birefringent filter (Lyot filter) was introduced into the cavity under a Brewster's angle.

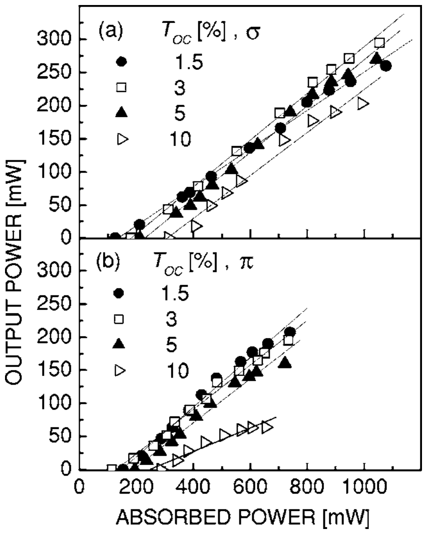

Fig. 7. Output power versus absorbed pump power of the Tm:NaGdW laser obtained with Ti:sapphire laser pumping for different transmission T_{OC} of the output coupler and (a) σ and (b) π polarization. The symbols show the experimental data and the linear fits (lines) were used to estimate the slope efficiency η and laser thresholds.

Table 5. Slope Efficiency η and Threshold P_{thr} Calculated with Respect to the Absorbed Pump Power and Laser Wavelength λ_L for Several Transmission Values T_{OC} of the Output Coupler Obtained for Room-Temperature cw Operation of the Tm:NaGdW Laser under Ti:sapphire Laser Pumping

	η (%)		λ_L (nm)		P_{thr} (mW)	
T_{OC} (%)	σ	π	σ	π	σ	π
1.5	29	33.5	1943	1943	126	114
3	35.3	37.4	1925	1925	182	153
5	34.9	33.2	1918	1917	212	194
10	32.4	17.7	1895	1896	312	286

polarizations, respectively. The Tm laser output was in the fundamental transversal mode. Figure 7 shows the output power versus absorbed pump power recorded for different output couplers. Optical damage occurred for an incident intensity exceeding ≈40 kW/cm^2. In the case of σ polarization, an output power of 295 mW was achieved for an absorbed power of 1054 mW. For π polarization, the maximum output reached 207 mW for an absorbed power of 740 mW. These two values were obtained with T_{OC} $=3\%$ and 1.5%, respectively. Table 5 summarizes the results for Ti:sapphire laser pumping. It can be seen that, although the maximum achievable output is much higher for the σ polarization due to the larger absorption, the efficiency in terms of absorbed pump power as well as the oscillation wavelengths are rather similar. The laser threshold in terms of absorbed power appears slightly lower for the π polarization. This behavior is in agreement with the spectral dependence of the gain cross sections calculated in Fig. 4, which is similar for the two polarizations. A systematic decrease of the laser wavelength with T_{OC} is observed, which is explained by the increased inversion rate as can be seen in Fig. 4. This is related to the stronger absorption bleaching at lower intracavity intensities.

The laser output power showed a slight tendency to roll over with increasing power for both polarizations. This is usually an indication of thermally induced population of the lower laser level. We studied the pump light absorption under laser operation and in the nonlasing state by interrupting the beam in one of the cavity arms (Fig. 8). As expected, the absorption is always higher for the σ polarization. In the low signal limit the absorption amounts to 75% and 50% for the σ and π polarizations, respectively, and these values drop in the nonlasing state to ~60% and 45%, respectively, due to the bleaching effect. At low values of T_{OC} the intracavity intensity increases the saturation intensity for the pump transition and the pump absorption increases correspondingly.[23] Nevertheless the small signal value is not reached even for T_{OC} $=1.5\%$. On the contrary, the effect is weaker for higher T_{OC}, and for $T_{\mathrm{OC}}=10\%$ and π polarization the dependence resembles the situation without lasing [see Fig. 8(b)].

Figure 9 shows the laser tunability achieved inserting a 3 mm thick quartz plate whose optical axis was at 60° to the surface (see Fig. 6). The tuning behavior was studied for both polarizations with $T_{\mathrm{OC}}=3\%$ using a fixed Ti:sapphire laser incident power of 1.54 W. The absorbed power was 1.05 and 0.74 W for the σ and π polarizations, respectively. The Tm:NaGdW laser wavelength was tunable from 1813 to 2025 nm in the case of σ polarization with a FWHM of 132 nm corresponding to ≈11 THz, and from 1817 to 1998 nm for the π polarization with a FWHM of 109 nm corresponding to ≈9 THz. The tunability limits achieved at the zero level for the σ polarization correspond to ≈17 THz. Such a full tuning range is one of the largest found in Tm^{3+}-doped solid-state lasers. While the

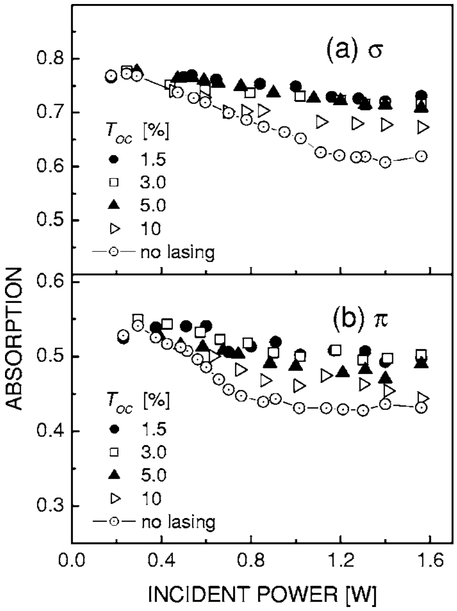

Fig. 8. Single-pass absorption of Tm:NaGdW under laser operation and without lasing versus incident pump power when pumped by the Ti:sapphire laser.

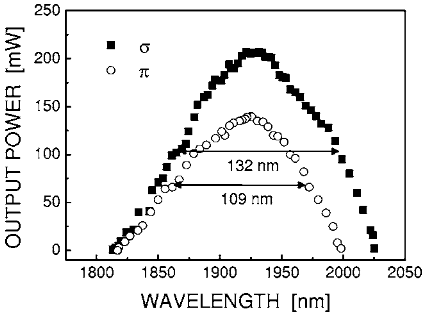

Fig. 9. Output power of the Tm:NaGdW laser versus wavelength for an incident power of 1.54 W of the Ti:sapphire pump laser and $T_{\mathrm{OC}}=3\%$.

tunability achieved with the ordered monoclinic Tm:KLu$(WO_4)_2$ using the same setup was only 10% narrower,[22] it should be outlined that in this case the crystal quality was much better and the maximum output level was above 1 W. This means that the results in this initial experiment with Tm:NaGdW can be regarded as optimistic. It can be expected that once the quality of Tm:NaGdW is also improved and the laser efficiency correspondingly increases, the tuning range will be even broader. The tuning range already achieved and in particular its smooth shape make us also optimistic concerning mode locking of Tm:NaGdW by passive methods and the generation of sub-100 fs pulses in the 2 μm spectral range by this laser.

B. Diode Laser Pumping

It is clear that power scaling of the Tm:NaGdW laser is not possible by Ti:sapphire laser pumping because of limitations related to the power of the primary green source. The wavelength of the available diode lasers is not always perfectly matched to the absorption profile for the specific host; however, since diode modules that provide more than 50 W are now commercially available, we also explored diode laser pumping of Tm:NaGdW.

For this purpose we used a diode laser module containing a single 50 W commercial bar with 19 emitters and a 30% fill factor, mounted in conduction-cooled packaging. More details about the pump source can be found elsewhere.[22] Only simple adapted beam shaping optics was used for the pump beam that was unpolarized (see Fig. 10). The nearly collimated beam had roughly a square cross section with a size of several millimeters. The emission wavelength could be tuned by temperature. At the maximum available output power of 20 W for the current power supply, the emission wavelength of the laser diode at room temperature was near 804.5 nm. However, for the present experiment the pump wavelength changed only from ~800 nm near threshold up to ~801 nm at the maximum incident power of 9.6 W applied. The single-peaked pump spectrum had a FWHM of ≈2 nm.

The same uncoated sample of Tm:NaGdW was tested in the nearly hemispherical cavity shown in Fig. 10. It was mounted in a water-cooled copper holder and the water temperature was maintained at 12 °C. The laser diode output was collimated by a collimating lens system with $f=34$ mm and 80% transmission and focused by a focusing lens system with $f=20$ mm and 88% transmission. The nearly circular spot achieved had a cross section with a diameter of ~125 μm.[22] M1 is a plane total reflector, and several output couplers (M2 in the figure) with different transmission T_{OC} were used.

The maximum output power achieved with the diode-pumped Tm:NaGdW laser and the $T_{\mathrm{OC}}=0.5\%$ output coupler was 330 mW when pumping with 9 W (incident power) corresponding to 4.5 W of absorbed pump power. The M^2 factor of the output (deviation from the fundamental transversal mode) was of the order of 2. In terms of absorbed pump power the threshold was 430 mW and the slope efficiency was 10%. The laser wavelength was 1997 nm in this case and got shorter for increasing T_{OC} as in the case of Ti:sapphire laser pumping. Compared with Table 5, however, it is clear that the increased oscillation wavelength and thresholds are a consequence of the lower gain and inversion rates. Since there were no polarization-selecting surfaces in this cavity, the laser selected the polarization only according to the higher gain and this was always the σ polarization. This is in agreement with the slightly better performance of this polarization in the Ti:sapphire laser-pumped configuration (Fig. 7), but it is difficult to see in Fig. 4 because the difference in the gain cross sections is rather small. Rollover in the power dependence can be clearly seen in Fig. 11. Also, the oscillation wavelength increased with the pump level and reached, e.g., for $T_{\mathrm{OC}}=0.5\%$, 2002 nm. The increase of the laser wavelength is a further indication of thermal effects that limit at present the performance of this laser. Note that reduction of the reabsorption losses at higher pump levels would, on the contrary, result in shorter oscillation wavelengths.

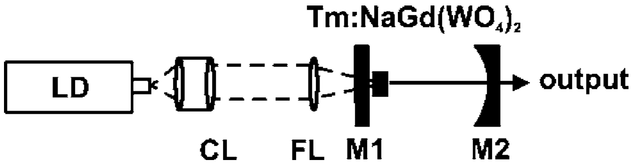

Fig. 10. Cavity setup of the laser diode- (LD-) pumped Tm:NaGdW laser. CL, collimating lens system; FL, focusing lens system; M1, plane total reflector; M2, output coupler with radius of curvature of −50 mm. Empty cavity length is 49 mm.

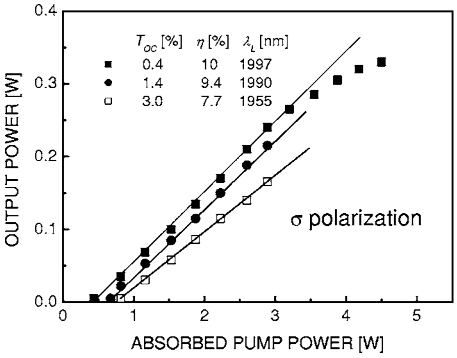

Fig. 11. Output power of the cw Tm:NaGdW laser under diode laser pumping versus absorbed pump power. The linear fits (lines) were used to calculate the slope efficiencies η corresponding to the three output couplers used. The oscillation wavelengths refer to operation near the threshold.

5. CONCLUSIONS

We successfully grew a disordered crystal of $NaGd(WO_4)_2$ doped with 5 mol.% Tm in the melt by the Czochralski method. The obtained concentration in the sample corresponded to 3.7 mol.%. Absorption and emission studies, both at low and room temperature, as well as lifetime measurements, provided the basic information necessary for understanding laser operation of Tm^{3+} in this host on the $^3F_4 \rightarrow {}^3H_6$ transition. We achieved tunable laser operation of Tm^{3+} in NaGdW near 2 μm pumping around 800 nm. To the best of our knowledge, this is the first time that room-temperature laser operation beyond the 1 μm spectral range characteristic of the Nd^{3+} and Yb^{3+} ions has been achieved with such disordered double tungstate or molybdate hosts.[24] The broad optical bands of these hosts are promising for tunable and mode-locked operation of Tm^{3+} lasers in the 2 μm spectral range and are suitable for pumping with AlGaAs laser diodes near 800 nm. The output powers achieved at room temperature in the cw regime ($\approx$300 mW) are modest but normal for this initial attempt to grow Tm:NaGdW. The laser gain is slightly higher for the σ polarization. This polarization also ensures a much higher pump efficiency. The continuous tunability obtained with an intracavity Lyot filter extends from 1813 to 2025 nm, one of the largest achieved with a Tm^{3+}-doped crystalline material, despite the relatively low efficiency obtained with this first sample of Tm:NaGdW. The congruent melting of NaGdW allows the growth of crystals with large size in a short time as required for profitable commercial applications. Considerable improvement in the laser performance can be expected after elimination of the internal refractive index gradients observed in the first grown crystal.

ACKNOWLEDGMENTS

We thank C. Kränkel and K. Petermann from Hamburg University for the pinhole measurement in Fig. 5. This work was supported within projects DT-CRYS or NMP3-CT-2003-505580 (European Union), and MAT2005-6354-C03-01 and MAT2004-21113-E (Spain). M. Rico (EX-2003-0784) and X. Mateos (EX-2004-1294) acknowledge the Education and Science Ministry of Spain for financial support.

The corresponding author is C. Zaldo. His e-mail address is cezaldo@icmm.csic.es.

REFERENCES

1. L. Bottrill, D. F. Perrault, Jr., M. M. Pankratov, and D. S. Poe, “Thulium:YAG laser applications for Stapes surgery: preliminary observations,” in *Laser Surgery: Advanced Characterization, Therapeutics, and Systems IV*, R. R. Anderson, ed., Proc. SPIE **2128**, 23–30 (1994).
2. R. M. Mihalcea, M. E. Webber, D. S. Baer, R. K. Hanson, G. S. Feller, and W. B. Chapman, “Diode-laser absorption measurements of CO_2, H_2O, N_2O, and NH_3 near 2.0 μm,” Appl. Phys. B **67**, 283–288 (1998).
3. W. Koechner, *Solid-State Laser Engineering* (Springer, 1996).
4. R. C. Stoneman and L. Esterowitz, “Efficient, broadly tunable, laser-pumped Tm:YAG and Tm:YSGG cw lasers,” Opt. Lett. **15**, 486–488 (1990).
5. P. Camy, J. L. Doualan, S. Renard, A. Braud, V. Menard, and R. Moncorge, “$Tm^{3+}:CaF_2$ for 1.9 μm laser operation,” Opt. Commun. **236**, 395–402 (2004).
6. P. Cornacchia, D. Parisi, E. Sani, A. Toncelli, and M. Tonelli, “Comparative analysis of the 2 μm emission in $Tm^{3+}:BaY_2F_8$ and $Tm^{3+}:KYF_4$: spectroscopy and laser experiment,” *Advanced Solid-State Photonics*, C. Denman and I. Sorokina, eds., Vol. 98 of OSA Trends in Optics and Photonics Series (Optical Society of America, 2005), pp. 219–223.
7. G. E. Peterson and P. M. Bridenbaugh, “Laser oscillation at 1.06 μm in the series $Na_{0.5}Gd_{0.5x}Nd_xWO_4$,” Appl. Phys. Lett. **4**, 173–175 (1964).
8. C. Cascales, M. D. Serrano, F. Esteban-Betegón, C. Zaldo, R. Peters, K. Petermann, G. Huber, L. Ackermann, D. Rytz, C. Dupré, M. Rico, J. Liu, U. Griebrier, and V. Petrov, “Structural, spectroscopic, and tunable laser performance of Yb^{3+}-doped $NaGd(WO_4)_2$,” Phys. Rev. B (to be published).
9. M. Rico, J. Liu, U. Griebner, V. Petrov, M. D. Serrano, F. Esteban-Betegón, C. Cascales, and C. Zaldo, “Tunable laser operation of ytterbium in disordered single crystals of $Yb:NaGd(WO_4)_2$,” Opt. Express **12**, 5362–5367 (2004).
10. L. Macalik, J. Hanuza, D. Jaque, and J. García-Solé, “Spectroscopic characterization of the Tm^{3+} doped $KLa(WO_4)_2$ single crystal,” Opt. Mater. **28**, 980–987 (2006).
11. X. Lu, Z. You, J. Li, Z. Zhu, G. Jia, B. Wu, and C. Tu, “Optical spectra of Tm^{3+} doped $NaBi(WO_4)_2$,” submitted to Opt. Mater.
12. L. D. Merkle, J. B. Gruber, M. D. Seltzer, S. B. Stevens, and T. H. Allik, “Spectroscopic analysis of $Tm^{3+}:NaLa(MoO_4)_2$,” J. Appl. Phys. **72**, 4269–4274 (1992).
13. E. Cavalli, C. Meschini, A. Toncelli, M. Tonelli, and M. Bettinelli, “Optical spectroscopy of Tm^{3+} doped in $KLa(MoO_4)_2$ crystals,” J. Phys. Chem. Solids **58**, 587–595 (1997).
14. E. Ya. Rode, V. N. Karpov, and M. M. Ivanova, “Influence of the rare-earth ion on the phases formed in the Na_2WO_4-$R_2(WO_4)_3$ systems (where R is a rare-earth element),” Russ. J. Inorg. Chem. **16**, 905–908 (1971) [translated from Z. Neorg. Khim. **16**, 1713–1716 (1971)].
15. P. C. Becker, T. Hayhurst, G. Shalimoff, J. G. Conway, N. Edelstein, L. A. Boatner, and M. M. Abraham, “Crystal field analysis of Tm^{3+} and Yb^{3+} in YPO_4 and $LuPO_4$,” J. Chem. Phys. **81**, 2872–2878 (1984).
16. C. Cascales, A. Méndez-Blas, M. Rico, V. Volkov, and C. Zaldo, “The optical spectroscopy of lanthanides R^{3+} in $ABi(XO_4)_2$ $(A=Li,Na;X=Mo,W)$ and $LiYb(MoO_4)_2$ multifunctional single crystals: relationship with the structural local disorder,” Opt. Mater. **27**, 1672–1680 (2005).
17. S. A. Payne, L. L. Chase, L. K. Smith, W. L. Kway, and W. F. Krupke, “Infrared cross-section measurements for crystals doped with Er^{3+}, Tm^{3+}, and Ho^{3+},” IEEE J. Quantum Electron. **28**, 2619–2630 (1992).
18. D. E. McCumber, “Einstein relations connecting broadband emission and absorption spectra,” Phys. Rev. **136**, A954–A957 (1964).
19. C. Görller-Walrand and K. Binnemans, “Spectral intensities of *f-f* transitions,” in *Handbook on the Physics and Chemistry of Rare Earths*, K. A. Gschneider, Jr., and L. Eyring, eds. (Elsevier Science, 1998), Vol. 25, p. 101.
20. W. T. Carnall, P. R. Fields, and K. Rajnak, “Electronic energy levels in trivalent lanthanide aquo ions. I: Pr^{3+}, Nd^{3+}, Pm^{3+}, Sm^{3+}, Dy^{3+}, Ho^{3+}, Er^{3+}, and Tm^{3+},” J. Chem. Phys. **49**, 4424–4442 (1968).
21. K. Petermann, D. Fagundes-Peters, J. Johannsen, M. Mond, V. Peters, J. J. Romero, S. Kutovoi, J. Speiser, and A. Giesen, “Highly Yb-doped oxides for thin-disc lasers,” J. Cryst. Growth **275**, 135–140 (2005).

22. X. Mateos, V. Petrov, J. Liu, M. C. Pujol, U. Griebner, M. Aguiló, F. Díaz, M. Galán, and G. Viera, "Efficient 2-μm continuous-wave laser oscillation of $Tm^{3+}:KLu(WO_4)_2$," IEEE J. Quantum Electron. 42, 1008–1015 (2006).
23. C. Lim and Y. Izawa, "Modeling of end-pumped cw quasi-three-level lasers," IEEE J. Quantum Electron. **38**, 306–311 (2002).
24. A. A. Kaminskii, "Modern developments in the physics of crystalline laser materials," Phys. Status Solidi A **200**, 215–296 (2003).